*Int. J. Heat Mass Transfer.* Vol. 36, No. 10, pp. 2635–2646, 1993
Printed in Great Britain

0017-9310/93 $6.00+0.00
Pergamon Press Ltd

# A measurement technique and a new model for the wall heat transfer coefficient of a packed bed of (reactive) powder without gas flow

M. PONS,† P. DANTZER‡ and J. J. GUILLEMINOT†

†CNRS-LIMSI, BP 133, 91403 Orsay Cedex, France
‡CNRS-URA 446, Bât, 415, Université Paris Sud, 91405 Orsay Cedex, France

(*Received* 19 *March* 1992 *and in final form* 15 *October* 1992)

**Abstract**—An experimental technique, designed for investigating altogether the effective thermal conductivity and the wall heat transfer coefficient in a packed bed of hydride powder, and the coupling of heat transfer with the hydriding reaction, is presented. It consists of measuring transient temperature evolution in a reactor with only geometrical symmetry and of fitting to the experimental data the numerical solution of the heat equation in the two-dimensional domain including the whole reactor. This method requires only a relatively small powder volume (30 $cm^3$). As a first step, results on non-reactive packed beds (500 $\mu$m glass beads with argon and 20 $\mu$m iron powder with hydrogen) validate the experimental technique. A new model for the wall heat transfer coefficient is developed for packed beds without gas flow. This model attempts to unify the current differing approaches of modeling this quantity. It predicts high values for small grain size and large variations in the Knudsen transition domain: this is qualitatively confirmed by experiments, with coefficients at around 3000 W $m^{-2}$ $K^{-1}$ being measured for 20 $\mu$m iron powder in hydrogen. Experimental results show that the pressure-dependent thermal resistances on wall and grain surfaces are not negligible.

## 1. INTRODUCTION

STUDIES of the thermal properties of micron size metallic powders have found growing interest during recent years in several domains. Our efforts have focused on hydrides, which represent a class of metallic compounds highly reactive to hydrogen gas. Hydrides look very attractive for applications such as hydrogen and energy storage, gas purification, isotopic separation or hydride batteries [1]. Hydride formation results from the solid state reaction of an alloy with hydrogen gas [1–9]. This transformation can be reversed, although undergoing an hysteresis, and the hydriding and de-hydriding reactions are both usually fast. The mechanical constraints generated by lattice volume expansion (around 20%) during hydrogen absorption transform the alloy into a fine powder (micron size grains) after a few hydriding–dehydriding cycles [2, 6–8]. This reaction is also strongly exothermic. Thus, the conditions for using the large quantity of hydrogen or energy (around 0.8 MJ $l^{-1}$) stored in hydrides are strongly correlated to the thermal behaviour of the packed bed. Measurement of the effective thermal conductivity, $\lambda_e$, and the wall heat transfer coefficient (WHTC), $\alpha_w$, of a $LaNi_5$ hydride power bed is the first goal of this work.

On the other hand, several authors have mentioned that the apparent reaction kinetics greatly depend on the experimental apparatus configuration and the sample thermal characteristics [2, 3, 8]. Investigation of the coupling between heat transfer and reaction within the sample is the second goal of this work.

The conductivity of packed beds has been very widely studied during the last decades. Different one-dimensional measurement techniques have been presented (steady-state or transient) [2, 5, 9–24], but they cannot be used for the dual purpose of our work. Furthermore, the experimental method must take two-dimensional effects in account, as done in ref. [25] (Section 2). Among the different models for the conductivity of packed beds [10–17, 26], we chose the one most adapted to our case. The heat transfer coefficient between the reactor wall and the bed (without gas flow) has been somewhat less investigated than the conductivity [13, 27–31]. A new model is proposed (Section 3). The experimental method validation is achieved by measuring $\lambda_e$ and $\alpha_w$ for the bed of 500 $\mu$m glass beads under an argon atmosphere. This bed was recently studied by Guilleminot *et al.* [24], so results of the present method can be compared with that previous work. The bed of 20 $\mu$m iron powder under hydrogen atmosphere, more closely resembled a hydride powder bed; the solid is metallic, the grains are micron size and the gas is hydrogen. This bed is the last calibration-step before studying $LaNi_5$, which is reactive. Results on both inert beds are presented in Section 4, and results on the hydride bed (involving reaction) will be presented in a future paper.

## NOMENCLATURE

$a$ thermal diffusivity of the packed bed [$m^2 s^{-1}$]
$B$ factor which defines the shape of a theoretical grain modelled in the ZBS model and in the present WHTC model
$C_p$ specific heat of the packed bed material [$J kg^{-1} K^{-1}$]
$C_s$ Stefan–Boltzmann constant [$W m^{-2} K^{-4}$]
$D_g$ average grain diameter in the packed bed [m]
$ei_{(j)}$ thickness of insulation associated with discretization element $j$ [m]
$e_{ir}$ hemispherical emissivity of solid material in the infra-red domain
$Gr$ Grashof number for ambient air above the reactor lid
$j$ number of an element in discretization of the reactor
$Kcv$ constant term in the expression of natural convection coefficient [$m^{-1}$]
$M^+_{lid}$ extra mass associated with reactor lid, due to attachments [kg]
$Pr$ Prandtl number for ambient air above the reactor lid
$Se_{(j)}$ external wall area for external discretization element $j$ [$m^2$]
$Si_{(j)}$ surface (averaged between $Se_{(j)}$ and external) area of insulation for external element $j$ [$m^2$]
$S_l$ total horizontal surface area of electrical heating [$m^2$]
$t$ time [s]
$T$ temperature [K]
$We$ electrical heating power [W]
$x, z$ coordinates of the theoretical grain surface.

Greek symbols

$\alpha_{gf}$ heat transfer coefficient corresponding to the thermal resistance at the grain solid surface [$W m^{-2} K^{-1}$]
$\alpha_w$ heat transfer coefficient between the reactor wall and packed bed [$W m^{-2} K^{-1}$]
$\alpha^0_w$ residual heat transfer coefficient (under vacuum) [$W m^{-2} K^{-1}$]
$\alpha_{wf}$ heat transfer coefficient corresponding to the thermal resistance at the wall solid surface [$W m^{-2} K^{-1}$]
$\gamma$ accomodation factor of the gas in the packed bed
$\delta$ roughness dimension [m]
$\Delta T$ temperature difference between the wall and distance $D_g/2$ [K]
$\Delta Ti$ temperature difference at the interface wall-packed bed [K]
$\Delta Te_{(j)}$ difference between the external wall temperature of element $j$ and the ambient temperature [K]
$\varepsilon$ packed bed porosity
$\varepsilon_w$ average porosity in the vicinity of the wall
$\varphi$ flattening coefficient at solid–solid contacts
$\Theta_0, \Theta_1, \Theta'_0$ temperatures generated in the wall vicinity by a unit flux density
$\lambda$ thermal conductivity of stainless steel [$W m^{-1} K^{-1}$]
$\lambda_a$ thermal conductivity of ambient air [$W m^{-1} K^{-1}$]
$\lambda_e$ effective thermal conductivity of the packed bed [$W m^{-1} K^{-1}$]
$\lambda'_e$ equivalent thermal conductivity of packed bed in the wall vicinity [$W m^{-1} K^{-1}$]
$\lambda^0_e$ residual effective thermal conductivity of the bed (under vacuum) [$W m^{-1} K^{-1}$]
$\lambda_g$ thermal conductivity of the gas phase in the packed bed [$W m^{-1} K^{-1}$]
$\lambda^*_g$ thermal conductivity of gas, modified by the Knudsen effect [$W m^{-1} K^{-1}$]
$\lambda_i$ thermal conductivity of the insulation [$W m^{-1} K^{-1}$]
$\lambda_s$ thermal conductivity of the solid phase in the packed bed [$W m^{-1} K^{-1}$]
$\rho$ apparent volumetric mass of the packed bed [$kg m^{-3}$]
$\sigma$ mean free path of gas molecules in the packed bed at pressure P [m]
$\nabla$ Vectorial gradient operator.

Abbreviations

WHTC · wall heat transfer coefficient
YKS Yagi, Kunii and Smith
ZBS Zehner, Bauer and Schlünder.

## 2. CHOICE OF AN EXPERIMENTAL TECHNIQUE

### 2.1. *Previous techniques*

The first and most well established method of determining the conductivity consists of measuring a stationary temperature gradient in a 'one-dimensional' volume of material, usually cylindrical [5, 10–15, 17, 21–23]. $\lambda_e$ is directly deduced from the temperature gradient, and $\alpha_w$ can also be evaluated when the wall temperature is measured. But 'steady-state' also means 'no reaction', so coupling of heat transfer

with reaction obviously cannot be investigated with this technique. Some transient methods are well known, such as the hot wire, probe, flash techniques [18–20, 24]. The hot wire technique is quite common, because an analytical solution of the Fourier equation can be achieved when the investigated material is 'one-dimensional', infinite (or large enough) and not reactive. More recent studies use a numerical solution (one-dimensional, finite difference scheme) [20, 24], and the conductivity is yielded by identification (fitting the numerical solution to the experimental data).

The study of a reactive material (e.g. solid–gas reaction) with a transient technique raises specific problems. First consequence: the Fourier equation must now include a source term corresponding to reaction, then it can only be solved numerically. Second consequence: two-dimensional effects cannot be neglected. It has been shown [25] that heating an adsorbent bed in a closed volume induces migration of adsorbate; vapor is desorbed from warmer parts of the bed and is transferred to colder parts, where it is adsorbed. Due to the heat of reaction, this migration induces a significant heat transfer parallel to conduction. The local adsorbed/desorbed quantity is strongly correlated with heat flux paths in the bed, which cannot be one-dimensional in the whole bed because of end effects. Consequently, the Fourier equation must be solved in the whole bed volume. Also, for calculating the heat fluxes at the bed boundaries, the model must include the whole reactor.

This procedure has additional benefits, $\lambda_e$ and $\alpha_w$ can be investigated in actual conditions. Finally, removing the one-dimensional condition allows the sample volume to be reduced. That is, given that the sample radius (e.g. cylindrical) must be much larger than a hot-wire or thermocouple diameter (around 1 mm), i.e. at least 20 mm, and given that the one-dimensional condition requires a sample with a minimal aspect ratio (height : radius) of 5, thus the minimal 'one-dimensional' sample volume lies around 100–130 $cm^3$, whereas the sample volume for our system is only 30 $cm^3$. This feature may be important for rare or expensive materials, and additionally, the reactor design may be more convenient, e.g. with respect to problems of tightening and sealing (a crucial point for hydrides and other materials highly sensitive to impurities).

Consequently the method presented herein is a combination of a cylindrical reactor without any one-dimensional constraint and a numerical model solving the Fourier equation in the whole reactor (two-dimensional domain). With this approach, values of $\lambda_e$ and $\alpha_w$ are obtained by identification. As a first step, this method is validated by studying inert beds, therefore only the model without a source term is presented herein.

### 2.2. *Experimental set-up*

A schematic of the reactor is presented in Fig. 1. It is composed of two parts made of 316-L stainless steel: a cylindrical body (inner diameter: 50 mm, outer diameter: 58 mm, inner height: 18 mm) and a lid (diameter: 90 mm, thickness: 10 mm). The packed bed is 10–16 mm deep, according to the filling. The bed top is not in contact with the reactor lid to allow free expansion of the hydride. An electrical resistance (Thermocoax, 1 mm diameter) is embedded into concentric circular furrows at the reactor bottom. Welded just underneath, a 1 mm thick circular copper sheet homogenizes the input heat flux. The reactor is largely insulated except on the lid.

Adequate instrumentation is required for determination of different heat flux paths in the reactor. Twelve ultrafast thermocouples (Type K, 0.5 mm

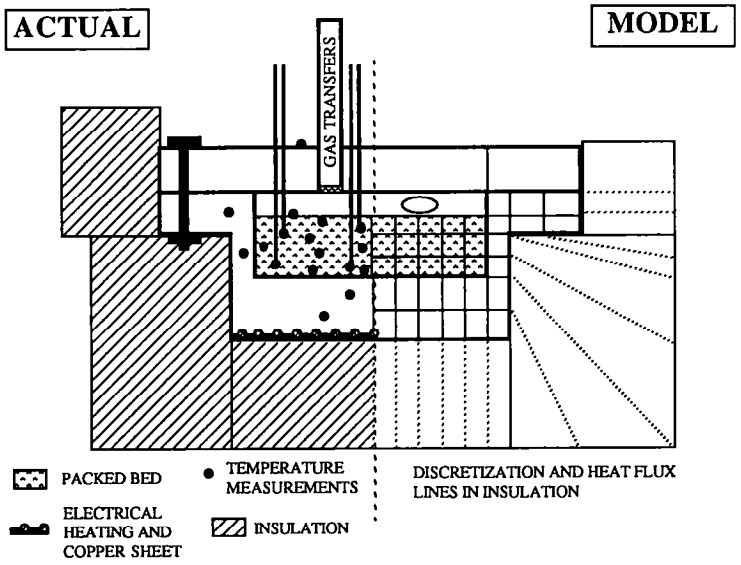


FIG. 1. Schematic of the measurement reactor and its discretization for modelling.

diameter, stainless steel sheath) are axially and radially distributed in the bed. They are installed through a tube fitting for vacuum and high pressure (Conax). Five other thermocouples are located in different places in or on the reactor walls. The positions of the internal thermocouples are measured with respect to the lid (±0.5 mm). The gas pressure in the reactor is measured by a pressure transducer, Heise, 0–2.5 MPa, (±0.05%).

The thermocouples are connected to a data acquisition system, Mess MDP 82 (±0.1 K). The voltage at the ends of the electrical heating resistance is measured by a multimeter, Keithley K175 (±0.1%). The MDP 82, K175 and pressure gauge are connected to a microcomputer, Kontron Ψ80, which also controls the heating power via the MDP 82.

The reactor tightness towards vacuum ($10^{-4}$ Pa) and hydrogen pressure of more than 3 MPa was tested. The reactor is connected by a bellows valve (3 MPa, Selfa) to either a diffusion pump for vacuum, or a gas injection system. 'Ultra pure' quality gases, argon and hydrogen, were provided by Air Liquide (France).

### 2.3. *Reactor model*

We present here only the model without reaction. Its main assumption is that the bed is a homogeneous medium, which is justified because there is no natural convection within it. Indeed, the modified Rayleigh number $Ra^*$, as defined in ref. [32], is always much lower than the critical value of $4\pi^2$.

The Fourier equation applies with uniform diffusivity in each continuous part of the system (the reactor body, lid and bed)

$$\frac{\partial T}{\partial t} = \nabla \cdot (a \cdot \nabla T). \tag{1}$$

The boundary conditions depend on the location of the considered element.

Symmetry of the reactor ensures adiabaticity at the central axis. For elements on the lid, heat losses by natural convection on lid top are evaluated according to ref. [33], which yields

$$-\lambda \cdot \left.\frac{\partial T}{\partial n}\right|_{\text{top}} = Kcv\, \lambda_a \cdot (Gr\, Pr)^{0.25} \cdot \Delta Te_{(j)} \tag{2}$$

where $\Delta Te_{(j)}$ is the difference between the external wall temperature for element $j$ and the ambient temperature. $Gr$ is calculated with $\Delta Te_{(j)}$, and $Pr$ and $\lambda_a$ are calculated for air at an average temperature between the ambient and wall temperature. The connecting tubes fixed on reactor lid are accounted for in factor $Kcv$ and also by increasing the mass of the lid central element by a quantity $M^+_{\text{lid}}$.

All other external discretization elements, except the lowest ones of the reactor bottom, are submitted to heat loss through the insulation. This yields:

$$-\lambda \cdot \left.\frac{\partial T}{\partial n}\right|_{\text{edge}} = \frac{\lambda_i \cdot Si_{(j)} \cdot \Delta Te_{(j)}}{ei_{(j)} \cdot Se_{(j)}}. \tag{3}$$

$Si_{(j)}$ and $ei_{(j)}$ are evaluated with the assumed flux lines through insulation shown in Fig. 1. $Se_{(j)}$ is the external wall area for element $j$. The insulation sensible heat is taken into account by increasing the heat capacity of the external reactor elements by a corresponding quantity.

Electrical heating takes place in the lowest elements of the reactor bottom. For these elements $Se_{(j)}$ equals $Si_{(j)}$ (see flux lines in Fig. 1), and equation (3) transforms into:

$$-\lambda \cdot \left.\frac{\partial T}{\partial n}\right|_{\text{bottom}} = \frac{\lambda_i \cdot \Delta Te_{(j)}}{ei_{(j)}} - \frac{We}{S_1}. \tag{4}$$

Heat transfer between the reactor body and the bed is represented by a third kind of boundary condition applied to the interface:

$$-\lambda_e \cdot \left.\frac{\partial T}{\partial n}\right|_{\text{interface}} = \alpha_w \cdot \Delta Ti. \tag{5}$$

The left-hand term (which defines the flux density through the interface) states that the local conductivity in the wall vicinity is the conductivity of the bed, $\lambda_e$. The WHTC, $\alpha_w$, is defined by the right hand term, where $\Delta Ti$ is the temperature jump which takes place at the bed–wall interface.

Heat transfer between the reactor body and the lid is also represented by a third kind of boundary condition, similar to equation (5), but with a heat transfer coefficient denoted by $\alpha_{\text{lid}}$. Calculation of the heat transfer through the cavity between the bed top and the lid takes in account gaseous conduction and infra-red radiation.

From a numerical point of view, the model uses the central finite difference Crank–Nicholson scheme with the discretization presented in Fig. 1. It evaluates by itself the computation time step required to limit the error induced by the linearization of the differential equations. The computation time-steps are short (1–2 s) when the temperature evolution is strongly transient and long (200 s) when the temperature evolution is quasi-linear. After each computation time-step, the model checks that the reactor global heat balance is correct.

The different parameters of the model are: $K_{cv}$, $M^+_{\text{lid}}$, $\alpha_{\text{lid}}$, $\rho \cdot C_p$ of the bed, $\alpha_w$ and $\lambda_e$. The three first parameters are experimental constants and do not depend on the bed. They are determined from a first set of experiments performed with an empty reactor, i.e. either evacuated or filled with argon or hydrogen alone. Once they are determined, the same values are used for all the packed beds. When the bed is defined ($\rho \cdot C_p$, $\alpha_w$ and $\lambda_e$ are prescribed), the input data for the model are the same as for experiments: sequence in time of the heating power and the ambient temperature.

### 2.4. *Identification procedure*

Each identification is performed on a set of three transient experiments scanning different regimes

Table 1. Conditions for the three transient experiments

| Experiment | Period: | 1 | 2 | 3 | 4 |
|---|---|---|---|---|---|
| 1 | Heating power: | 8.9 W | 22.8 W | 2.8 W | 0 W until back |
| | during: | 8 min | 8 min | 10 min | to ambient |
| 2 | Heating power: | 15.3 W | 8.9 W | 0 W | |
| | during: | 10 min | 8.5 min | until back to ambient | |
| 3 | Heating power: | 22.8 W | 3.6 W | | |
| | during: | 8.5 min | until steady-state | | |

(heating, cooling and evolution toward steady-state) and different changes in heating/cooling rate to separate the effects of the different parameters. These experimental conditions are described in Table 1. The precision of the identified values is deduced by comparison of the model sensitivity with the experimental temperature measurement accuracy. Typical results of identification are presented in Fig. 2 for one of the studied beds.

## 3. INTERPRETATION MODELS

Once values of $\lambda_e$ and $\alpha_w$ are identified, it is worthwhile investigating their different components (gaseous conduction, solid conduction, radiation ...) and the Knudsen effect. This is achieved with experiments at different gas pressures, and with the help of interpretation models for the conductivity and WHTC.

### 3.1. *Effective thermal conductivity model*

The most famous models for the effective thermal conductivity of packed beds have been developed by Yagi, Kunii, Smith *et al.* [10–15, 27] (denoted herein by 'YKS model'), and by Zehner, Bauer, Schlünder *et al.* [16, 17, 24, 27, 34], ('ZBS model'). Both assume that heat flux paths in the bed are parallel at the macroscopic and microscopic scales. Both models are phenomenological and require the experimental value of the residual conductivity (conductivity of the bed in a vacuum). They are easy to use and they apply quite well to most randomly packed beds, with an accuracy of about 30%. Both of the models estimate contributions of the continuous gas phase, of the solid phase at contact points, of the alternation of gas and solid around contact points, and of radiation. Also, both take the Knudsen effect into account. The YKS model considers spherical grains, the number of contact points between them depending on porosity. It

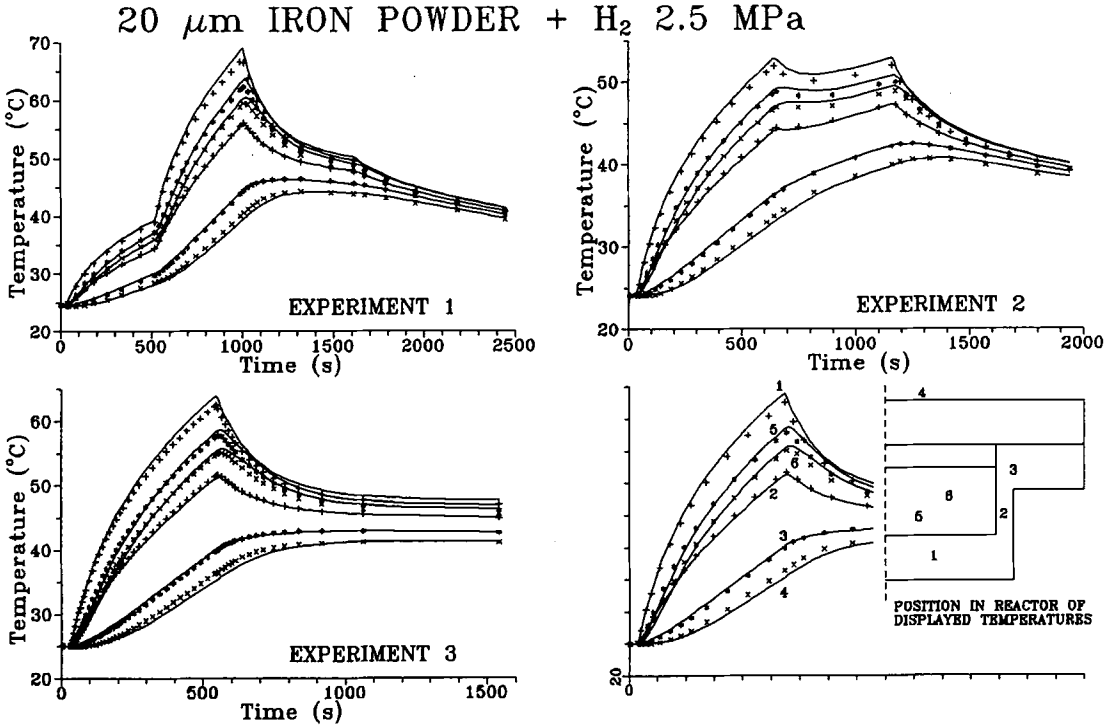


FIG. 2. Presentation of the three experiments performed for each identification and a typical example of the calculated temperatures (curves) fitted to measurements (points).

also assumes that all spheres have same diameter. The ZBS model represents grains by a theoretical particle, the shape of which depends on the bed porosity, the shape of real grains and the diameter distribution. The ZBS model applies to different types of grains, especially 'broken material', and also to grains of different diameters. Therefore it will be used herein for further study. This model is explained in Appendix 1.

### 3.2. *Wall heat transfer coefficient model*

The heat transfer between a wall and a material contacting it has been widely represented by empirical global heat transfer coefficients. But, in numerical modelling, boundary conditions must not be confused with equations in the bulk of the material. The latter involve the heat transfer resistances of the material (effective thermal conductivity and geometry). The former involve resistances at the wall–material interface, represented by the wall heat transfer coefficient (WHTC), $\alpha_w$. In addition, a better understanding of these resistances will permit optimizing. As a further step, knowledge of the WHTC of packed beds requires modelling as advanced as for effective thermal conductivity.

In order to model the WHTC of beds without gas flow, Bauer [27, 28] and more recently Schlünder and Tsotsas [29] calculated the thermal resistance in the gas between the wall and spherical grains contacting it, accounting for the Knudsen effect. Temperature is implicitly assumed to be uniform in the solid grain, i.e. the solid conductivity, $\lambda_s$, is much larger than the gaseous conductivity, $\lambda_g$. This is then equivalent to calculating the thermal resistance from the wall to a distance $D_g/2$ in the bed, with a negligible thermal resistance in the solid. These authors state that the WHTC is the inverse of this thermal resistance. When the temperature gradient in the vicinity of the wall is considered (Fig. 3), the thermal resistance between the wall and a distance $D_g/2$ from it, is represented by the temperature difference $(\Theta_0-\Theta_1)$ in Fig. 3. But the WHTC, $\alpha_w$, as defined by equation (5), is correlated, not with $(\Theta_0-\Theta_1)$, but with $(\Theta_0-\Theta'_0)$, where $\Theta'_0$ is the result of extrapolation of the temperature gradient within the bed (slope $-\lambda_e^{-1}$) up to the wall, see Fig. 3. Then, if we denote by $\lambda'_e$ the equivalent thermal conductivity that would yield $(\Theta_0-\Theta_1)$ on distance $D_g/2$, $\{\lambda'_e = 0.5\cdot D_g\cdot(\Theta_0-\Theta_1)^{-1}\}$, the WHTC is defined by:

$$\alpha_w = \frac{2\cdot\lambda_e}{(\lambda_e/\lambda'_e-1)\cdot D_g}. \tag{6}$$

Suzuki's recent analysis also agrees with equation (6) [35].

Let us comment further on equation (6). It is well known that from the wall to a distance $D_g/2$, the local porosity is much larger than within the bed refs. [36–38]. Usually, the conductivity is less in the gas than in the solid, so $\lambda'_e$ is smaller than $\lambda_e$. Thus the larger porosity near the wall induces a thermal resistance, represented by the coefficient $\alpha_w$. As can be seen in equation (6), $\alpha_w$ is inversely proportional to $D_g/2$. This is so because $D_g/2$ is the distance on which local conductivity is less than $\lambda_e$, and it can also be seen from Fig. 3 that $(\Theta_0-\Theta'_0)$ is proportional to $D_g/2$.

Let us now consider a packed bed of insulating grains in a better conducting gas (e.g. $H_2$ or He). The increased porosity near the wall will induce $\lambda'_e$ to be larger than $\lambda_e$. According to equation (6), $\alpha_w$ would then be negative. This does not mean that the heat flux is in the inverse direction of the temperature gradient. This only means that one point in the bed has better heat transfer with the wall than with any other point in the bed at the same distance from it. This also means that the present definition of the wall heat transfer coefficient, $\alpha_w$, is completely different from the usual convective heat transfer coefficient, which is defined using the temperature difference between the wall and a reference (at infinity for a slab, or average temperature for a tube). These considerations also lead to the conclusion that $(\alpha_w)^{-1}$ would be a more relevant concept; it represents an additional thermal resistance due to presence of the wall instead of continuity of the bed. The advantages of this concept are: (1) it avoids confusion with global heat transfer coefficient, (2) negative values are not paradoxical, (3) it can be compared with the resistance of the bed itself. Anyway, in the presently studied beds, $\lambda_s$ is much larger than $\lambda_g$ ($\alpha_w > 0$), so we will still use the common concept of the transfer coefficient $\alpha_w$.

Finally, one can guess that the $\lambda_e$ and $\lambda'_e$ values are rather close; the quantity $(\lambda_e/\lambda'_e-1)$ appearing in equation (6) will depend greatly upon the value of $\lambda'_e$, and for its correct evaluation the thermal resistance in the solid grain surely cannot be neglected [31, 35]. In our model for $\alpha_w$, $\lambda'_e$ is derivated with the same approach as in the ZBS model for $\lambda_e$. As a consequence, some figures, such as grain flattening at contact points, must be the same for both $\lambda_e$ and $\alpha_w$ evaluations. In addition, the ZBS grain may be spherical: influence of the model assumptions on $\alpha_w$ will be evaluated by comparing results with the ZBS particle and with the spherical grain.

The derivation of our model for $\lambda'_e$, given in Appendix 2, yields:

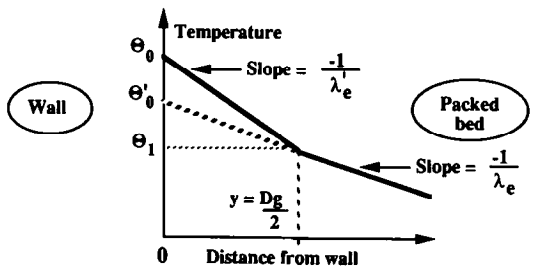


FIG. 3. Schematic representation of the temperature gradient (per unit heat flux density) in the wall vicinity.

$$\lambda_e' = \left\{\varphi\cdot\sqrt{(1-\varepsilon_w)}\cdot\lambda_s+(1-\sqrt{(1-\varepsilon_w)})\right.$$
$$\cdot\frac{\varepsilon_w\cdot\lambda_g\cdot D_g}{2\cdot\Lambda+\varepsilon_w\cdot D_g}+(1-\varphi\cdot\sqrt{(1-\varepsilon_w)})$$
$$\cdot\frac{2\cdot e_{ir}}{2-e_{ir}}\cdot C_s\cdot T^3\cdot D_g+\frac{(1-\varphi)\cdot\sqrt{(1-\varepsilon_w)}\cdot\lambda_g\cdot B}{\left(1-\frac{\lambda_g}{\lambda_s}\right)\cdot Z_2}$$
$$\left.\cdot\left[\frac{1-B}{B}-\frac{2}{Z_2}-\frac{2\cdot Z_1'}{Z_2^2}\cdot\ln\left(1-\frac{Z_2}{Z_1'}\right)\right]\right\} \quad (7)$$

with

$$Z_1' = 1+2\cdot\Lambda/D_g \quad (8)$$

and

$$Z_2 = B-Z_1'\cdot(B-1). \quad (9)$$

Factor $B$ defines the theoretical grain shape; when $B = 1$, the grain is spherical. $\Lambda$ is the mean free path of gas molecules at the prescribed pressure, modified by the accommodation factor $\gamma$ (cf. ref. [16, 17])

$$\Lambda = \sigma\cdot(2-\gamma)/\gamma.$$

Once $\lambda_e$ and $\lambda_e'$ are calculated, $\alpha_w$ is yielded by equation (6). As the dependence of $\alpha_w$ on $D_g$ has been mentioned, we present it in Fig. 4 for a bed of glass beads under argon, with $D_g$ lying between 50 $\mu$m and 5 mm. We present also the experimental $\lambda_e$ and $\alpha_w$ values from ref. [24], where $D_g$ equals 500 $\mu$m, and

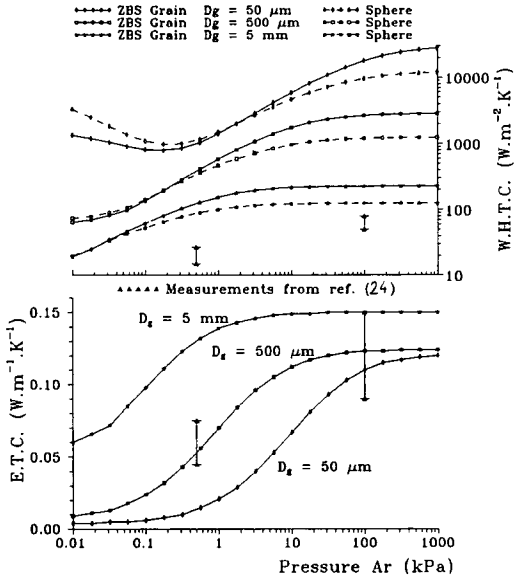


FIG. 4. Influence of grain diameter $D_g$ on the calculated effective thermal conductivity (ETC) $\lambda_e$ and the calculated wall heat transfer coefficient (WHTC) $\alpha_w$ (glass beads with argon, $D_g$ = 50, 500 $\mu$m, or 5 mm); ▲: measurements from ref. [24] with experimental precision ($D_g$ = 500 $\mu$m); ETC curves; ZBS model; WHTC curves: our model either with a ZBS grain (full lines) or with a spherical grain (dashed lines) (both diagrams have same $X$-axis).

the curves of conductivities calculated with the ZBS model, that show the position of Knudsen transition domain. Without the Knudsen effect (e.g. $P = 1$ MPa), the calculated $\alpha_w$ is indeed inversely proportional to $D_g$. Because of the Knudsen effect it can vary by more than an order of magnitude, and can be very low at low pressure. But for small grains (50 $\mu$m), the low limit at low pressure disappears, and the $\alpha_w$ curve only shows a minimum around 1000 W m$^{-2}$ K$^{-1}$. In this case, the Knudsen effect affects $\lambda_e$ and $\lambda_e'$ similarly. Also, the difference between the ZBS particle and the spherical grain is a factor of 2–3, which is still less than the total variation, then the calculated range of magnitude does not depend on the model assumptions.

Finally, it appears in Fig. 4 that the calculated values of $\alpha_w$ with $D_g$ = 500 $\mu$m are much larger than the experimental ones. It is the same for our measurements on this bed and on iron powder with hydrogen. Consequently, we deduce that another thermal resistance exists between the wall and the contacting grains. Schlünder and Tsotsas propose the concept of roughness on the grain surface: the mean free path, $\Lambda$, would be enhanced by the size of the rough patch, $\delta$ [29]. When derivating the thermal resistance between the wall and contacting grain, increasing $\Lambda$ by $\delta$ is equivalent to adding a $\delta$ thick gas layer between the wall and grain, but at the contact point. Indeed, for small grains (20–500 $\mu$m diameter) the roughness effect may not be negligible, and these rough patches may enclose some gas, creating a thermal resistance on the grain surface. But, firstly, if the grain surface roughness is accounted for, so the wall surface roughness must be. Secondly, recent works showed the fractal nature of rough surfaces (e.g. ref. [39]) then the roughness size is not unique. Therefore, instead of one geometrical quantity, only attached to the grain, we propose the concept of thermal resistances located on the grain- and wall surfaces, i.e. on the solid surfaces. As already mentioned, the concept of thermal resistances is more relevant, but for the sake of consistency with the concept of transfer coefficient, we represent these resistances by 'solid surface heat transfer coefficients': $\alpha_{wf}$ for the wall surface and $\alpha_{gf}$ for the grain surface, that are inserted in each transfer mode between the wall and the contacting grain. With these coefficients, equations (7)–(9) transform into

$$\lambda_e' = \left\{\varphi\cdot\sqrt{(1-\varepsilon_w)}\cdot\frac{\lambda_s\cdot\alpha_{wf}\cdot\alpha_{gf}\cdot D_g}{(\alpha_{wf}+\alpha_{gf})\cdot 2\cdot\lambda_s+D_g\cdot\alpha_{wf}\cdot\alpha_g}\right.$$
$$+(1-\varphi\cdot\sqrt{(1-\varepsilon_w)})\cdot 2\cdot\frac{e_{ir}}{2-e_{ir}}\cdot C_s\cdot T^3\cdot D_g$$
$$+(1-\sqrt{(1-\varepsilon_w)})\cdot\frac{\varepsilon_w\cdot\lambda_g\cdot D_g}{2\cdot\Lambda+\varepsilon_w\cdot\left(D_g+2\cdot\frac{\lambda_g}{\alpha_{wf}}\right)}$$
$$+\frac{(1-\varphi)\cdot\sqrt{(1-\varepsilon_w)}\cdot\lambda_g\cdot B}{\left(1-\frac{\lambda_g}{\lambda_s}\right)\cdot Z_2}$$

$$\cdot\left[\frac{1-B}{B}-\frac{2}{Z_2}-\frac{2\cdot Z_1}{Z_2^2}\cdot\ln\left(1-\frac{Z_2}{Z_1}\right)\right]\Bigg\} \quad (10)$$

with

$$Z_1=\frac{\frac{\lambda_g}{\alpha_{wf}}+\frac{\lambda_g}{\alpha_{gf}}+\frac{D_g}{2}+\Lambda}{\frac{D_g}{2}\cdot\left(1-\frac{\lambda_g}{\lambda_s}\right)} \quad (11)$$

and

$$Z_2=B-Z_1\cdot(B-1). \quad (12)$$

The details of this derivation are presented in Appendix 2. Figure 5 presents the individual influences of $\alpha_{wf}$ (or $\alpha_{gf}$) on $\alpha_w$ calculated with equations (6), (10)–(12), for the bed of 500 $\mu$m glass beads under argon, $\alpha_{wf}$ and $\alpha_{gf}$ have almost the same influence on $\alpha_w$. This can easily be seen in equation (10), where $\alpha_{wf}$ and $\alpha_{gf}$ are symmetrical except for transfer by gas only (third term on the right-hand side). It also appears that measurements from ref. [24] correspond to $\alpha_{gf}$ values lying between 10 and 100 W m$^{-2}$ K$^{-1}$. If these values were translated in terms of roughness dimension $\delta$ ($\delta=\lambda_g/\alpha_{gf}$), $\delta$ would lie between 160 and 1600 $\mu$m. Obviously, this cannot correspond to roughness on 500 $\mu$m diameter beads. In addition $\alpha_{gf}$ is pressure dependent when $\delta$ should be constant.

In the following, the $\alpha_w$ model is used for determination of $\alpha_{wf}$ and $\alpha_{gf}$ in different experimental cases. As their respective influences cannot be distinguished, we state that $\alpha_{wf}=\alpha_{gf}$, and determine the value that makes $\alpha_w$, calculated with equations (6), (10)–(12), equal to the experimental value. It can be noted that $\alpha_{wf}$, which is attached to the wall, should depend only on gaseous phase and not on solid material.

Finally, the present definition and model for $\alpha_w$ are very useful for evaluation of the steady-state temperature gradient within the bed, according to

$$\Theta_0-\Theta=1/\alpha_w+y/\lambda_e \quad (13)$$

where $\Theta_0-\Theta$ is the temperature difference between the wall and distance $y$ from it, for a unit flux density. And increasing the heat transfer efficiency of a packed bed is equivalent to reducing $\Theta_0-\Theta$.

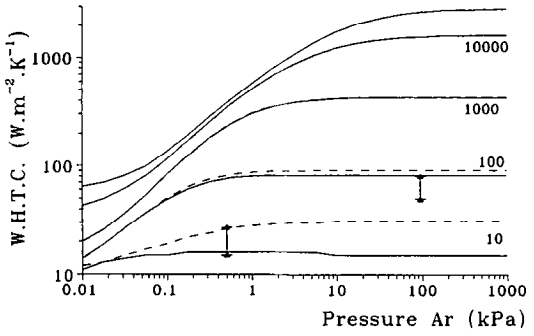


FIG. 5. Individual influences of $\alpha_{wf}$ and $\alpha_{gf}$ on the calculated WHTC $\alpha_w$; ▲: measurements from ref. [24]; upper curve: model without solid surface resistance; solid lines: $\alpha_w$ model for $\alpha_{wf}$ lying between 10 and $10^4$ W m$^{-2}$ K$^{-1}$ and for infinite $\alpha_{gf}$; dashed lines: $\alpha_w$ model for $\alpha_{gf}$ lying between 10 and $10^4$ W m$^{-2}$ K$^{-1}$ and for infinite $\alpha_{wf}$.

## 4. EXPERIMENTAL RESULTS AND DISCUSSION

The characteristics of the studied packed beds are described in Appendix 3. Their porosity, $\varepsilon$, has been measured.

### 4.1. 500 $\mu$m glass beads under argon atmosphere

Figure 6 presents identified values of $\lambda_e$ and $\alpha_w$ as functions of pressure together with model predictions. Results from ref. [24] are also shown for comparison.

The experimental values are identified with a precision of $\pm 50\%$, which can be explained by two effects. Firstly, this bed has a rather low conductivity and WHTC, consequently, at least 95% of the heat input passes through the reactor walls (4 mm thick) and less than 5% passes through the bed. Thus a small inaccuracy on the heat balance over the whole reactor is amplified when considering the flux passing through the bed alone. Secondly, the internal thermocouples and glass beads have the same diameter, thus contact between them may be poor, and also the thermocouple sheathes have a much larger thermal conductivity than the bed. The temperature measurements may be slightly biased. This particular bed represents the lower bounds of what can be measured with this reactor. Simple technical modifications, such as reduction of the wall thickness, would easily remedy this problem. Nevertheless, the identified values are consistent with results from ref. [24] and with the $\lambda_e$

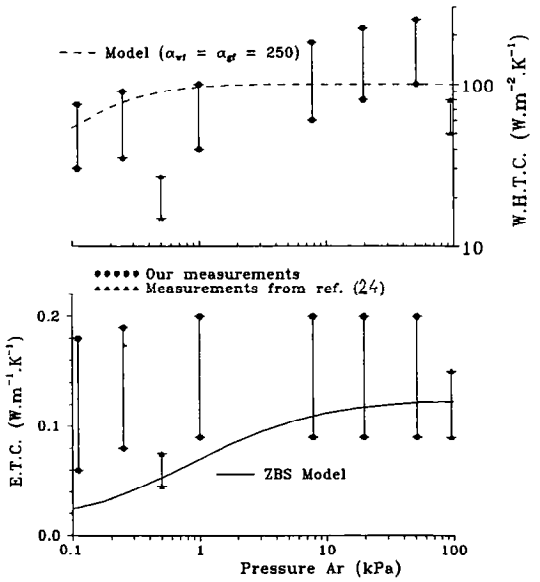


FIG. 6. Effective thermal conductivity and wall heat transfer coefficient for the packed bed of 500 $\mu$m glass beads + argon. ●: our measurements; ▲: measurements from ref. [24]; curves: models (both diagrams have same $X$-axis).

Table 2. Values of $\alpha_{wf}$ ($=\alpha_{gf}$) introduced in the WHTC model for adjustment on identified $\alpha_w$: 500 $\mu$m glass beads with argon

| Pressure (kPa) | 0.11 | 0.25 | 1.0 | 7.8 | 19.6 | 51.2 |
|---|---|---|---|---|---|---|
| $\alpha_{wf}$ ($\alpha_{gf}$) mini | 65 | 65 | 70 | 130 | 180 | 250 |
| $\alpha_{wf}$ ($\alpha_{gf}$) maxi | 210 | 240 | 260 | 570 | 750 | 900 |

model predictions for argon pressure of more than 10 kPa. Despite the above-mentioned restriction, the experimental technique still appears to be valid.

The values of $\alpha_{wf}$ ($=\alpha_{gf}$) yielded by comparison between identified WHTC's and our $\alpha_w$ model are presented in Table 2. The 'mini–maxi' range corresponds to precision on $\alpha_w$.

### 4.2. 20 $\mu$m *iron powder under hydrogen atmosphere*

For granulometry determination, iron powder produced by Merck, F.R.G., was passed through sieves. Fifty percent was found to lie between 20 and 30 $\mu$m, and 50% under 20 $\mu$m. According to the definition of the average grain diameter, $D_g$, described in ref. [16], $D_g$ lies in the range 15–25 $\mu$m.

Identified values of the conductivity and WHTC are presented in Fig. 7, as are the predictions of the models. The problems encountered with the glass beads partially vanish. Both solid material and gas are now more conductive; then the proportion of total heat input passing through the bed lies around 15%. Furthermore, the solid grains are much smaller than the thermocouples. As a result, the precision of identified values is $\pm 20\%$, which is the same order of magnitude as the claimed accuracy of the ZBS model. The identified values of conductivity and predictions

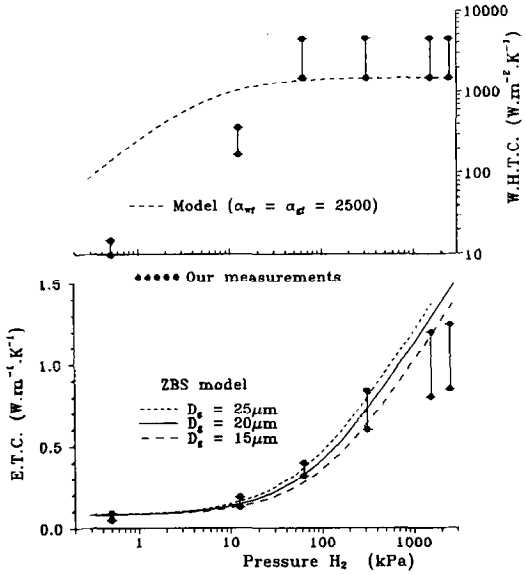


FIG. 7. Effective thermal conductivity and wall heat transfer coefficient for the packed bed of 20 $\mu$m iron powder + hydrogen: ●: measurements, curves: models (both diagrams have same $X$-axis).

by models are quite consistent. Evolution of the WHTC shows interesting features. $\alpha_w$ can be very large: 3000 W m$^{-2}$ K$^{-1}$ (which is the upper limit our device can detect), and it changes by several orders of magnitude when pressure is reduced. At 500 Pa, $\alpha_w$ practically collapses to 13 W m$^{-2}$ K$^{-1}$. These experimental results qualitatively confirm some trends of our model: very large $\alpha_w$ for small grains, and a large variation in the Knudsen transition domain.

The values of $\alpha_{wf}$ (set equal to $\alpha_{gf}$) yielded by comparison between the identified $\alpha_w$ and our WHTC model are presented in Table 3. Here again, they are pressure dependent and when these solid surface heat transfer coefficients are transformed in terms of roughness, the minimum value would be 23 $\mu$m, i.e. larger than grain diameter.

## 5. CONCLUSION

Determination of fine powder heat transfer parameters, the effective thermal conductivity and the wall heat transfer coefficient (WHTC), can be performed with a 'two-dimensional' method, that requires a sample volume of only 30 cm$^3$. This method is especially designed for studying reactive materials. Parameters are obtained by fitting the experimental temperature measurements with a numerical two-dimensional model of the whole reactor. The reactor intrinsic thermal characteristics are determined by preliminary experiments with an empty reactor. Good accuracy of identification requires thermocouple diameters larger than the grain sizes, and a sufficient proportion of heat input passing through the packed bed. Results on two inert beds (500 $\mu$m glass beads with argon and 20 $\mu$m iron powder with hydrogen) are satisfactory. A following paper will present results on $LaNi_5$ powder with either argon (inert bed) or hydrogen (reactive bed).

Bauer, Schlünder and Tsotsas on the one hand [27, 29], and Suzuki on the other hand [35] have proposed two different definitions and models for the WHTC $\alpha_w$. Our model attempts to unify the approaches developed by these different authors. Like Suzuki, we consider the WHTC to apply strictly to the interface between the wall and bed. For calculating heat transfer in the vicinity of the wall, we transform the model developed by Zehner, Bauer, Schlünder *et al.* for conductivity and adapt it for prediction of the WHTC.

Some characteristics of this model are qualitatively confirmed by experimental values for 20 $\mu$m iron powder under hydrogen atmosphere. Because of the small

Table 3. Values of $\alpha_{wf}$ ($=\alpha_{gf}$) introduced in the WHTC model for adjustment on identified $\alpha_w$: 20 $\mu$m iron powder with hydrogen

| Pressure (kPa) | 0.5 | 12.5 | 62.5 | 312 | 1550 | 2500 |
|---|---|---|---|---|---|---|
| $\alpha_{wf}$ ($\alpha_{gf}$) mini | 8 | 280 | 2700 | 2500 | 2500 | 2500 |
| $\alpha_{wf}$ ($\alpha_{gf}$) maxi | 16 | 660 | 10000 | 8450 | 8250 | 8250 |

grain diameter, when the pressure is above the Knudsen transition domain, the WHTC can be very large, around 3000 W $m^{-2}$ $K^{-1}$. When the pressure is lowered, the WHTC undergoes a tremendous variation; down to 13 W $m^{-2}$ $K^{-1}$. Furthermore, the present work on the WHTC seems to indicate that thermal resistances exist on the wall- and grain-surfaces. These solid surface thermal resistances (herein represented by 'solid surface heat transfer coefficient') are pressure-dependent, and they cannot be explained by a prescribed roughness dimension $\delta$, as done in ref. [29]. This is consistent with recent work showing the fractal nature of rough surfaces.

*Acknowledgements*—This work was supported by C.N.R.S. through A.R.C. TRANSTHERM (contract No. 8880: 09/03/1988). Authors specially thank F. Marcelet for his contribution on the data acquisition system.

## REFERENCES

1. P. Dantzer, Progress in metal-hydride technology, to appear in *Tropics in Applied Physics, Hydrogen in Metals, III* (Edited by H. Wipf). Springer (likely 1993).
2. P. D. Goodell, Thermal conductivity of hydriding alloy powders and comparisons of reactor systems. *J. Less-Common Met.* **74,** 175–184 (1980).
3. P. S. Rudman, Hydriding and dehydriding kinetics, *J. Less-Common Met.* **89,** 93–110 (1983).
4. A. Bernis and A. Stock, Stockage de l'hydrogène sous forme d'hydrures dans un réacteur à lit fixe on fluidisé, *Entropie* **116/117,** 58–63 (1984).
5. E. Suissa, I. Jacob and Z. Hadari, Experimental measurements and general conclusions on the effective thermal conductivity of powdered metal hydrides, *J. Less-Common Met.* **104,** 287–285 (1984).
6. P. Dantzer, Static, dynamic and cycling studies on hydrogen in the intermetallics $LaNi_5$ and $LaNi_{4.77}Al_{0.22}$, *J. Less-Common Met.* **131,** 349–363 (1987).
7. J. E. Bonnet, P. Dantzer, H. Dexpert, J. M. Esteva and R. Karnatak, Modifications near the surface owing to hydrogen cycling of the intermetallics $LaNi_5$ and $LaNi_{5-x}Al_x$, *J. Less-Common Met.* **130,** 491–495 (1987).
8. C. Bayane and N. Gerard, Kinetics study by thermogravimetry: the role of heat transfer, of sample mass and of sample holder design on metal hydride kinetics results, *Thermochimica Acta* **103,** 51–56 (1986).
9. E. Bershadsky, Y. Josephy and M. Ron; Permeability and thermal conductivity of porous matrix hydride compacts, *J. Less-Common Met.* **153,** 65–78 (1989).
10. D. Kunii and J. M. Smith, Heat transfer of porous rocks, *A.I.Ch.E. Jl* **6,** 71–78 (1960).
11. G. P. Willhite, D. Kunii and J. M. Smith, Heat transfer in beds of fine particles (Heat transfer perpendicular to flow), *A.I.Ch.E. Jl,* **8,** 340–345 (1962).
12. S. Masamune and J. M. Smith, Thermal conductivity of beds of spherical particles, *I & EC Fundam.* **2,** 136–143 (1963).
13. K. Ofuchi and D. Kunii, Heat transfer characteristics of packed beds with stagnant fluid, *Int. J. Heat Mass Transfer* **8,** 749–757 (1965).
14. T. Koya and D. Kunii, Measurement of effective thermal conductivities of solid particles in packed beds, *Int. Chem. Eng.* **12,** 162–167 (1972).
15. H. Sahnoune and Ph. Grenier, Mesure de la conductivité thermique d'une zéolithe, *Chem. Eng. J.* **40,** 45–54 (1989).
16. R. Bauer and E. U. Schlünder, Effective radial thermal conductivity of packing in gas flow: Part II: thermal conductivity of the packing fraction without gas flow, *Int. Chem. Engng* **18,** 189–204 (1978).
17. E. Tsotsas and H. Martin, Thermal conductivity of packed beds: a review, *Chem. Engng Proc.* **22,** 19–37 (1987).
18. A. K. Singh, R. Singh and D. R. Chaudhary, Prediction of effective thermal conductivity of moist porous materials, *J. Phys. D: Appl. Phys.* **23,** 698–702 (1990).
19. S. P. Rooke and R. E. Taylor, Transient experimental technique for the determination of the thermal diffusivity of fibrous insulation, *J. Heat Transfer* **110,** 270–273 (1988).
20. B. W. Jones, Thermal conductivity probe: development of method and application to a coarse granular medium, *J. Phys. E: Sci. Instrum.* **21,** 832–839 (1988).
21. A. B. Duncan, G. P. Peterson and L. S. Fletcher, Effective thermal conductivity with packed beds of spherical particles, *J. Heat Transfer* **111,** 830–836 (1989).
22. M. Nagel, Y. Komazaki and S. Suda, Effective thermal conductivity of a metal hydride bed augmented with a copper wire matrix, *J. Less-Common Met.* **120,** 35–43 (1986).
23. S. Suda, Y. Komazaki and N. Kobayashi, Effective thermal conductivity of metal hydride beds, *J. Less-Common Met.* **89,** 317–324 (1983).
24. J. J. Guilleminot and J. Gurgel, Heat transfer intensification in absorbent beds of adsorption thermal devices, *Solar Engineering 1990, Proc. 12th Annual Int. Solar Energy Conf., Miami, Apr. 1990,* pp. 69–74, (Edited by J. T. Beard and M. A. Ebadian). A.S.M.E. New York, (1990).
25. J. J. Guilleminot, F. Meunier and J. Pakleza, Heat and mass transfer in a non-isothermal fixed bed solid adsorbent reactor: a uniform pressure, non uniform temperature case, *Int. J. Heat Mass Transfer* **30,** 1595–1606 (1987).
26. S. Hayashi, K. Kubota, H. Masaki, Y. Shibata and K. Takahashi, A theoretical model for the estimation of the effective thermal conductivity of a packed bed of fine particles, *Chem. Engng J.* **35,** 51–60 (1987).
27. R. Bauer, Stagnant packed beds. In *Heat Transfer to Gas–Solid Systems,* Chap. 2.8.1, pp. 1–15. Hemisphere, New York (1983).
28. E. Muchowski, Packed and agitated beds. In *Heat Transfer to Gas-Solid Systems,* Chap. 2.8.3, pp. 1–10. Hemisphere, New York (1983).
29. E. U. Schlünder and E. Tsotsas, *Wärmeübertragung in Festbetten, durchmischten Shüttgütern und Wirbelschichten,* Chap. 2, pp. 71–89. G. Thieme, Stuttgart (1988).
30. G. P. Peterson and L. S. Fletcher, Thermal contact conductance of packed beds in contact with a flat surface, *J. Heat Transfer* **110,** 38–41 (1988).
31. J. J. Guilleminot, Transfert de chaleur dans les lits granulaires, *A.R.C. Transtherm report,* C.N.R.S. PIRSEM, Paris (1990).
32. N. Kladias and V. Prasad, Natural convection in horizontal porous layers: effects of Darcy and Prandtl numbers, *J. Heat Transfer* **111,** 926–935 (1989).
33. W. H. McAdams, *Heat Transmission,* Chap. 7.3. McGraw-Hill, New York (1954).
34. M. Pons and P. Dantzer, Effective thermal conductivity in hydride packed beds: I: study of basic mechanisms, *J. Less-Common Met.* **172–174,** 1147–1156 (1992).
35. M. Suzuki, Heat transfer parameters in packed beds. In *Adsorption Engineering,* pp. 193–197. Kodansha (Tokyo) and Elsevier (Amsterdam) (1990).
36. K. Ridgway and K. J. Tarbuck, The random packing of spheres, *Br. Chem. Engng* **12,** 384–388 (1967).
37. L. H. S. Roblee, R. M. Baird and J. W. Tierney, Radial porosity variation in packed beds, *A.I.Ch.E. Jl.* **4,** 460–464 (1958).
38. R. F. Benenati and C. B. Brosilow, Void fraction dis-

tribution in beds of spheres, *A.I.Ch.E. Jl* **8**, 359–361 (1962).
39. A. Majumdar and C. L. Tien, Fractal network model for contact conductance, *ASME J. Heat Transfer* **113**, 516–525, (1991).

## APPENDIX 1: ZBS MODEL FOR PACKED BED EFFECTIVE THERMAL CONDUCTIVITY $\lambda_e$

The effective conductivity is the sum of transfers through the continuous gaseous phase (with Knudsen effect) + infra-red radiation, the solid phase (via contact points between grains), and the solid in series with the gaseous phases (with Knudsen effect) + infra-red radiation [16, 17]:

$$\lambda_e = \left\{(1-\sqrt{(1-\varepsilon)})\cdot\varepsilon\cdot\left[\frac{\lambda_g}{\varepsilon+\frac{\Lambda}{D_g}}+\lambda_{ir}\right] + \sqrt{(1-\varepsilon)}\cdot[\varphi\cdot\lambda_s+(1-\varphi)\cdot\lambda^*_{so}]\right\}$$

with

$$\lambda_{ir} = 4\cdot C_s\cdot D_g\cdot\frac{e_{ir}}{2-e_{ir}}\cdot T^3$$

$$\lambda^*_{so} = \frac{2}{M}\cdot\left\{\frac{B\cdot(\lambda_s+\lambda_{ir}-\lambda_g)\cdot\lambda_g\cdot\left(1+\frac{\Lambda}{D_g}\right)}{M^2\cdot\lambda_s}\right.$$

$$\cdot\ln\frac{(\lambda_s+\lambda_{ir})\cdot\left(1+\frac{\Lambda}{D_g}\right)}{B\cdot\left[\lambda_g+\frac{\Lambda}{D_g}\cdot(\lambda_s+\lambda_{ir})\right]}-\frac{B-1}{M}\cdot\lambda_g$$

$$\left.\cdot\left(1+\frac{\Lambda}{D_g}\right)+\frac{B+1}{2\cdot B}\cdot\left[\lambda_{ir}\cdot\left(1+\frac{\Lambda}{D_g}\right)-B\cdot\left(\lambda_g+\frac{\Lambda}{D_g}\cdot\lambda_{ir}\right)\right]\right\}$$

where

$$M = \left[1+\frac{\lambda_{ir}}{\lambda_s}-\frac{B\cdot\lambda_g}{\lambda_s\cdot\left(1+\frac{\Lambda}{D_g}\right)}\right]\cdot\left(1+\frac{\Lambda}{D_g}\right)-B\cdot\frac{\Lambda}{D_g}\cdot\left(1+\frac{\lambda_{ir}}{\lambda_s}\right).$$

## APPENDIX 2: OUR MODEL FOR PACKED BED WALL HEAT TRANSFER COEFFICIENT $\alpha_w$

According to equation (6), $\alpha_w$ depends on $\lambda_e$ and on $\lambda'_e$, which is the equivalent thermal conductivity between the wall and distance $D_g/2$. The present modeling of $\lambda'_e$ takes into account:

—an isotherm at the wall, and an isotherm at distance $D_g/2$, the temperature difference between them is $\Delta T$,
—parallel flux lines between these two isotherms,
—an average porosity between the wall and distance $D_g/2$, equal to $\varepsilon_w$,
—heat transfer coefficients $\alpha_{wf}$ and $\alpha_{gf}$ corresponding to thermal resistances located on the wall and grain surfaces (the expression without these resistances is simply deduced from present result),
—heat transfer through the solid phase (via contact points), through the continuous gas phase, through the gas and solid in series; each transfer is multiplied by a coefficient calculated from $\varepsilon_w$ with exactly same expressions as in the ZBS model of conductivity [16, 17],
—heat transfer by infra-red radiation, assumed to be parallel to all other ones, and to take place between surfaces that are not in contact,
—a flattening factor $\varphi$ at the contact points, as defined in ref. [16, 17].
—a theoretical grain shape with same expression as in the ZBS model of conductivity, i.e.

$$x^2+\frac{z^2}{[B-(B-1)z]^2}=1. \tag{A1}$$

Shape factor $B$ depends on $\varepsilon_w$ through:

$$B = C_{form}\cdot\left(\frac{1-\varepsilon_w}{\varepsilon_w}\right)^{10/9} \tag{A2}$$

where $C_{form}=1.25$ for a monodisperse spherical packing and $C_{form}=1.4$ for a continuous granular distribution of broken solids [16, 17]. $\varepsilon_w$ is deduced from $\varepsilon$ by interpolation between extreme values of 0.476 for $\varepsilon=0.476$ (cubic loose packing) and of 0.395 for $\varepsilon=0.260$ (rhombedral packing). When $B=1$, the grain is spherical.

Transfer in the solid phase, through the contact surface area is:

$$\Phi_{ss} = \varphi\cdot\sqrt{(1-\varepsilon_w)}\cdot\frac{2\cdot\lambda_s\cdot\alpha_{wf}\cdot\alpha_{gf}}{(\alpha_{wf}+\alpha_{gf})\cdot2\cdot\lambda_s+D_g\cdot\alpha_{wf}\cdot\alpha_{gf}}\cdot\Delta T. \tag{A3}$$

Infra-red radiative transfer is

$$\Phi_{ir} = (1-\varphi\cdot\sqrt{(1-\varepsilon_w)})\cdot\frac{4\cdot e_{ir}\cdot C_s\cdot T^3}{2-e_{ir}}\cdot\Delta T. \tag{A4}$$

In this study, $(\Phi_{ir}/\Delta T)$ lies around 6 W m$^{-2}$ K$^{-1}$.

Using the same expression as in ref. [16, 17], heat transfer in the continuous gaseous phase is

$$\Phi_g = (1-\sqrt{(1-\varepsilon_w)})\cdot\frac{2\cdot\varepsilon_w\cdot\lambda_g}{2\cdot\Lambda+\varepsilon_w\cdot\left(D_g+2\cdot\frac{\lambda_g}{\alpha_{wf}}\right)}\cdot\Delta T \tag{A5}$$

where $\Lambda=\sigma\cdot(2-\gamma)/\gamma$.

Heat transfer through the solid and gas in series is integrated on the grain surface, which yields

$$\Phi_{sg} = \frac{4\cdot(1-\varphi)\cdot\sqrt{(1-\varepsilon_w)}\cdot\lambda_g\cdot B}{D_g\cdot\left(1-\frac{\lambda_g}{\lambda_s}\right)\cdot Z_2}\cdot\Delta T \cdot\left[\frac{1-B}{2\cdot B}-\frac{1}{Z_2}-\frac{Z_1}{Z_2^2}\cdot\ln\left(1-\frac{Z_2}{Z_1}\right)\right] \tag{A6}$$

with

$$Z_1 = \frac{\frac{\lambda_g}{\alpha_{wf}}+\frac{\lambda_g}{\alpha_{gf}}+\frac{D_g}{2}+\Lambda}{\frac{D_g}{2}\cdot\left(1-\frac{\lambda_g}{\lambda_s}\right)} \tag{A7}$$

and

$$Z_2 = B-Z_1\cdot(B-1). \tag{A8}$$

Equation (A6) is not defined for $Z_2=0$. A limit study shows that, when $Z_2=0$

$$\Phi_{sg} = \frac{4\cdot(1-\varphi)\cdot\sqrt{(1-\varepsilon_w)}\cdot\lambda_g\cdot B}{D_g\cdot\left(1-\frac{\lambda_g}{\lambda_s}\right)}\cdot\Delta T\cdot\left(\frac{3\cdot Z_1-1}{6\cdot Z_1^2}\right). \quad \text{(A9)}$$

For spherical grains, ($B = 1$), one has

$$\Phi_{sg} = \frac{4\cdot(1-\varphi)\cdot\sqrt{(1-\varepsilon_w)}\cdot\lambda_g}{D_g\cdot\left(1-\frac{\lambda_g}{\lambda_s}\right)}\cdot\Delta T\cdot\left[Z_1\cdot\ln\left(\frac{Z_1}{Z_1-1}\right)-1\right]. \quad \text{(A10)}$$

Finally, $\lambda_e'$ is yielded by

$$\lambda_e' = \frac{D_g}{2}\cdot\left(\frac{\Phi_{ss}+\Phi_{ir}+\Phi_g+\Phi_{sg}}{\Delta T}\right) \quad \text{(A11)}$$

which is explained in equation (10). A limit analysis for vanishing $(\alpha_{wf})^{-1}$ and $(\alpha_{gf})^{-1}$ yields equations (7)–(9). The WHTC, $\alpha_w$, is yielded by equation (6).

## APPENDIX 3: PHYSICAL CHARACTERISTICS OF REACTOR AND PACKED BEDS

—Reactor: 316-L stainless steel:
$\rho\cdot C_p = 3.76\ \text{MJ m}^{-3}\text{K}^{-1}$ $\lambda = 15\ \text{W m}^{-1}\text{K}^{-1}$.

—Glass beads + argon:
$\rho\cdot C_p = 1.20\ \text{MJ m}^{-3}\text{K}^{-1}$ mass of packed bed = 42.21 g.

Height of packed bed in reactor = 14.0 mm
$\varepsilon = 0.39\pm0.01$. $\varepsilon_w = 0.45$
$\lambda_s = 0.92\pm0.02\ \text{W m}^{-1}\text{K}^{-1}$ $\lambda_g = 0.016\ \text{W m}^{-1}\text{K}^{-1}$
$\lambda_e^0 = 0.007\ \text{W m}^{-1}\text{K}^{-1}$ $\alpha_w^0 = 8\ \text{W m}^{-2}\text{K}^{-1}$
$\gamma = 0.90$ $\varphi = 5.0\cdot10^{-3}$.

—Iron powder + hydrogen:
$\rho\cdot C_p = 2.00\ \text{MJ m}^{-3}\text{K}^{-1}$ mass of packed bed = 84.0 g

Height of packed bed in reactor = 10.0 mm
$\varepsilon = 0.45\pm0.01$ $\varepsilon_w = 0.47$
$\lambda_s = 80\ \text{W m}^{-1}\text{K}^{-1}$ $\lambda_g = 0.189\ \text{W m}^{-1}\text{K}^{-1}$
$\lambda_e^0 = 0.09\ \text{W m}^{-1}\text{K}^{-1}$ $\alpha_w^0 = 8\ \text{W m}^{-2}\text{K}^{-1}$
$\gamma = 0.15$ $\varphi = 1.5\cdot10^{-3}$.